PNAS
www.pnas.org

Supplementary Information for

Real-time dissection of dynamic uncoating of individual influenza viruses

Chong Qin, Wei Li, Qin Li, Wen Yin, Xiaowei Zhang, Zhiping Zhang, Xian-En Zhang, Zongqiang Cui*

*Corresponding author: Zongqiang Cui
Email: czq@wh.iov.cn

This PDF file includes:

Supplementary text
Figs. S1 to S7
Captions for movies S1 to S13

Other supplementary materials for this manuscript include the following:

Movies S1 to S13

Supporting Information Text

SI Materials and Methods

Plasmids. A cDNA-bidirectional transfection system for the generation of IAV was used in this study (1). Eight plasmids (pHW2000) contained all the cDNA of the virus A/Puerto Rico/8/34 (H1N1). The pHW2000 PA–AP tag was constructed to replace the WT PA segment and rescue the recombinant virus PR8 PA–AP. Briefly, the PA–AP segment was constructed by inserting a sequence encoding the short linker GSGG, a 15-amino acid biotin AP tag (Nucleic acid sequence: GGTCTGAACGATATCTTCGAGCTCAGAAAATCGAATGGCACGAA), and a duplication of 165 base pairs of the 3′ end of the PA-coding region after the PA ORF (stop codon deleted) using one-step sequence, ligation-independent cloning (2) as depicted in Fig. S1A. pCDNA3.1(+)-BirA was constructed to express biotin ligase BirA, and BirA catalyzed the linkage between the PA protein and biotin. pCDNA3.1-Nup153-Venus and pEGCP-Rab7 were used to label the NPC and late endosome, respectively.

Cell and viruses. Human embryonic kidney cells (293T) were maintained in Dulbecco's modified Eagle's medium (DMEM) with 10% fetal bovine serum (FBS). MDCK cells were grown in modified Eagle's medium (MEM) with 10% FBS. Viruses were grown in 10-day-old specific pathogen free (SPF) chicken embryos at 37 °C or in MDCK cells maintained in MEM with 0.3% bovine serum albumin (BSA) and 0.5 μg/ml TPCK-trypsin.

Reverse genetics for recombinant virus construction. PR8 PA–AP recombinant viruses were rescued using the eight-plasmid reverse genetics system by transfection in 293T cells with Lipofectamine® 2000 reagent (Invitrogen), after which they were plaque-purified in MDCK cells. Selected plaques were used to inoculate 10-day-old embryonated chicken eggs. Infectivity titers for all virus stocks were calculated as the $TCID_{50}$ per ml.

Production of IAV-QDs. MDCK cells were maintained in an environment with 5% CO_2 at 37 °C in MEM with 10% FBS. Eighteen hours before transfection, MDCK cells were seeded in 100-mm dishes. MDCK cells were transfected with 15.0 μg of pcDNA3.1(+)-BirA plasmid DNA using Lipofectamine® 2000 Reagent, and 50 μM biotin (Sigma Aldrich) was added to the cells at the same time. After 6 h of transfection, the cells were washed three times with phosphate-buffered saline (PBS), and rPR8 PA-AP viruses at a multiplicity of infection (MOI) of 10 were incubated with the cells for 1 h at 37 °C. Afterward, the medium was changed to MEM containing 0.3% BSA (Sigma Aldrich), tosylsulfonyl phenylalanyl chloromethyl ketone (TPCK)-trypsin, and 50 μM biotin (Sigma Aldrich). After a 2-h incubation, SA-QDs were delivered into MDCK cells by a second transfection using Lipofectamine® 2000 Reagent.

Virus purification. Cell culture supernatants were harvested every 12 h after virus infection, and cells were supplemented with fresh medium until 3 days post-infection. To remove cell debris, the collected supernatants were subjected to centrifugation at

8000 rpm for 10 min at 4 °C (Eppendorf 18965 rotor), filtered through a 0.45-μm filter (Milipore), and then concentrated by centrifugation at 28000 rpm at 4 °C for 2.5 h (Beckman SW32 rotor) on 5 ml of a 30% (w/v) sucrose cushion in PBS. The pellet was then layered onto a 20–60% sucrose density gradient, followed by centrifugation at 35000 rpm for 3.5 h at 4 °C with an SW41 rotor. Fractions containing QDs were collected under UV excitation and centrifugated at 23000 rpm for 1.5 h at 4 °C to remove sucrose. Purified virus was resuspended in PBS (pH 7.4) for further experiments.

Transmission electron microscopy. Samples were loaded onto carbon-coated copper grids; 5 min later, the redundant liquid was removed using filter papers. The grids were washed once with PBS and then negatively stained with 10 μl of 1% phosphotungstate for 20 s at room temperature. Prepared copper grids were examined under a transmission electron microscope (H-7000 FA, Hitachi).

Immunofluorescence and western blot analyses. Samples were overlaid on polylysine-coated coverslips for 60 min at 37 °C or incubated with MDCK cells in glass-bottomed dishes (Cellvis) for 30 min at 4 °C and then shifted to 37 °C for 10 min. The coverslips or glass-bottomed dishes were washed with PBS, fixed with 4% formaldehyde, permeabilized with 0.1% Triton X-100, and blocked with 10% FBS. The samples were incubated with mouse monoclonal antibody against M1 (Abcam) (1:500), HA (Sino Biological Inc) (1:500), or NP (Abcam) (1:200) at 37 °C for 1 h and then with

Alexa Fluor 488 or 647-labeled goat anti-mouse IgG (1:1000) (Cell Signaling Technology). Fluorescence was monitored with an Ultra View Vox confocal system (PerkinElmer, Co.) using a 60× objective lens. Virus-infected cells and purified viruses were treated with gel-loading buffer, and 10-μl samples were subjected to western blot analysis using specific antibodies and HRP-streptavidin. Signals were detected using a BeyoECL Plus kit (BeyoECL, China).

Viral envelope labeling by QDs. This method was performed as reported previously (3). Briefly, purified viruses were biotinylated through reaction with Sulfo-NHS-LC-Biotin (Thermo Fisher) (1:1) at room temperature for 2 h, followed by removal of unreacted Sulfo-NHS-LC-Biotin by NAP desalting columns (GE Healthcare). Biotinylated viruses were adsorbed onto MDCK cells through incubation at 4 °C followed by washing to remove free viruses. SA-QDs were added to react with the adsorbed viruses, after which the samples were washed again to remove unreacted SA-QDs and imaged under a confocal microscope.

Cellular component labeling and virus tracking. Subcellular structures were labeled through the transfection of MDCK cells with individual plasmids encoding ECFP-Rab7 or Venus-Nup153, and the cells were incubated at 37 °C for 24 h prior to imaging. For IAV imaging in live cells, MDCK cells were seeded onto 35-mm cell culture glass-bottomed dishes. IAV-QDs were incubated with the cells at a MOI of 10 or 100 for 30 min at 4 °C to synchronize virus entry. The culture dishes were then placed into the live

cell incubation chamber (at 37 °C and 5% CO_2) of a Nikon Ti-e microscope (Tokai Hit) to allow virus entry, and the virions were imaged using a 60× objective lens and excitation wavelengths of 405, 488, 561, and 640. The imaging data were analyzed using Volocity software.

Viral neutralization and drug inhibition analysis. For the neutralization experiment, 5 mg/ml anti-HA antibody was added to IAV-QDs and incubated for 1h at room temperature (4). Inhibitors were present in the infection medium at the following concentrations: NH_4Cl, 20 mM; amantadine, 100 μm; IPZ (Sigma), 100 μm; and LMB (Sigma), 40 ng/ml (5, 6). During drug inhibition analysis, MDCK cells were pretreated with these inhibitors of 1 h and then infected with IAV.

RT-qPCR. To measure viral entry kinetics, intracellular levels of NP mRNA were quantified at different time points post-infection by real-time qPCR as reported before (7). The temperature profile included RT reaction at 42 °C for 5 min, 95 °C for 10 s, and denaturation at 95 °C for 5 min, amplification in two steps at 95 °C for 10 s, and 62 °C for 20 s and a melting curve from 65 to 90 °C.

***In vitro* virus disassembly assay.** The *in vitro* disassembly assay of viral particles was performed as previously described (8). Briefly, purified virus was loaded on a two-layer glycerol gradient (15%-25%). The bottom layer contained NP-40, 150 mM NaCl and was adjusted to different pH by adding appropriate buffer. The same gradient setup was

used when NaCl was replaced with KCl. Gradients were centrifuged for 150 min at 21000 rpm. The pellet in the bottom dissolved in loading buffer was separated by SDS-PAGE.

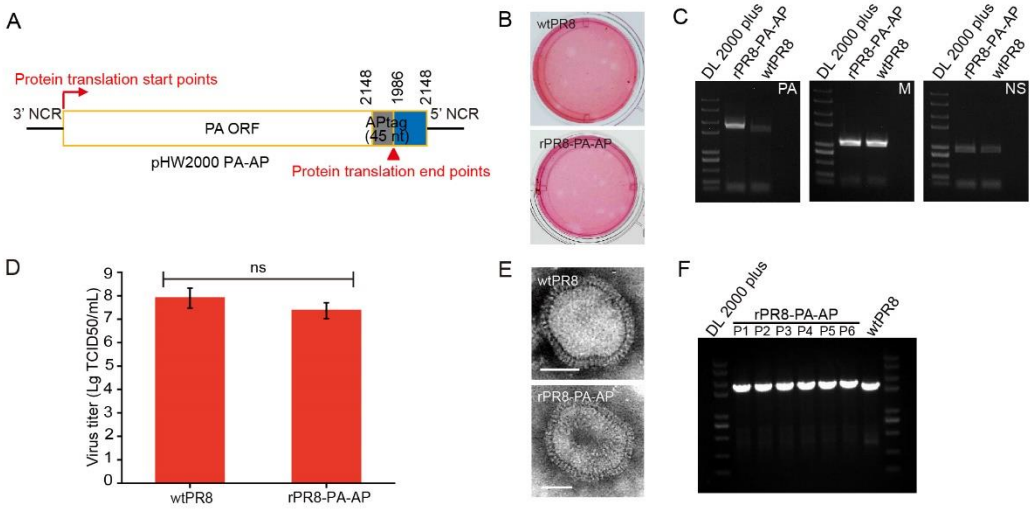

Fig. S1. Generation of rPR8-PA-AP influenza virus. (*A*) Schematic of the constructed plasmid pHW2000 PA-AP created by inserting the sequence of biotin AP into the C-terminal domain of the PR8 PA ORF. The 3′- and 5′-ends of the noncoding regions (NCR), and a duplication packaging sequence (163 nts in the PA-coding region from position 1986 to 2148) (blue), which is responsible for the efficient incorporation of vRNA into virus particles. The AP tag sequence (gray) was inserted between the PA gene and the 163 nt duplication packaging sequence. Protein translation start points (→) and stop points (▲) are shown. (*B*) wtPR8 virus (up) and rPR8-PA-AP virus (down) plaques on MDCK cells. (*C*) RT-PCR detection of PA (left), M (middle), and NS (right) from allantoic fluid. (*D*) Titers in PFU/ml of WT PR8 and rPR8-PA-AP after 48 h of growth in embryonated eggs at 37 °C. ns, not significant. (*E*) Negative staining of purified rPR8-PA-AP; scale bar: 50 nm. (*F*) Viral genome stability analysis. rPR8-PA-AP virus were consecutively incubated on MDCK cells for 6 passages. PA-AP gene was detected using RT-PCR.

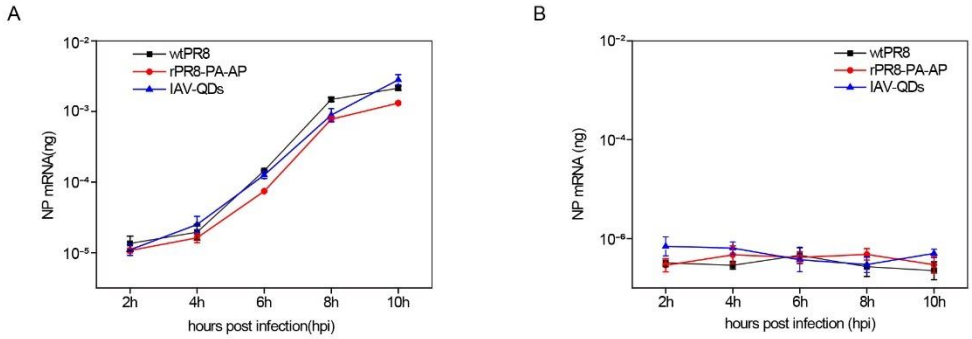

Fig. S2. Entry kinetics of IAV-QDs. (*A*) MDCK cells were infected with wtPR8, rPR8-PA-AP and IAV-QDs at an MOI of 10 and harvested at indicated time points. (*B*) Cells treated with NH_4Cl were infected with wtPR8, rPR8-PA-AP and IAV-QDs at an MOI of 10 and harvested at indicated time points. The viral NP mRNA were measured by RT-qPCR, n=3.

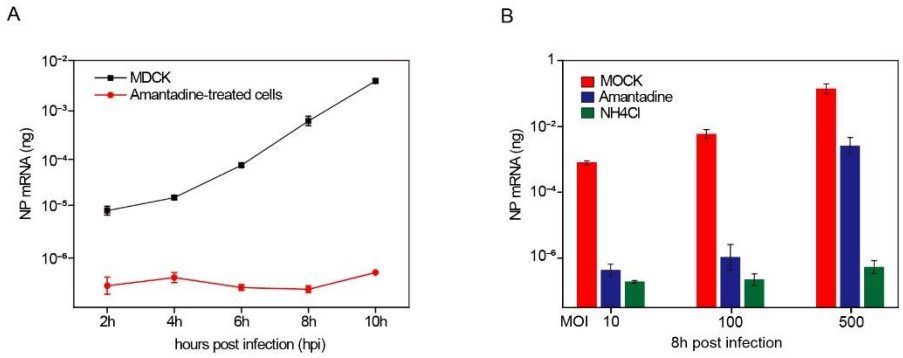

Fig. S3. Amantadine inhibition assay on rPR8-PA-AP entry. (*A*) MDCK cells or amantadine-treated cells were infected with wtPR8, rPR8-PA-AP and IAV-QDs at an MOI of 10 and harvested at indicated time points. (*B*) Cells treated with amantadine or NH_4Cl were infected with rPR8-PA-AP at MOI of 10, 100 and 500 and harvested at 8h post infection. The viral NP mRNA were measured by RT-qPCR, n=3.

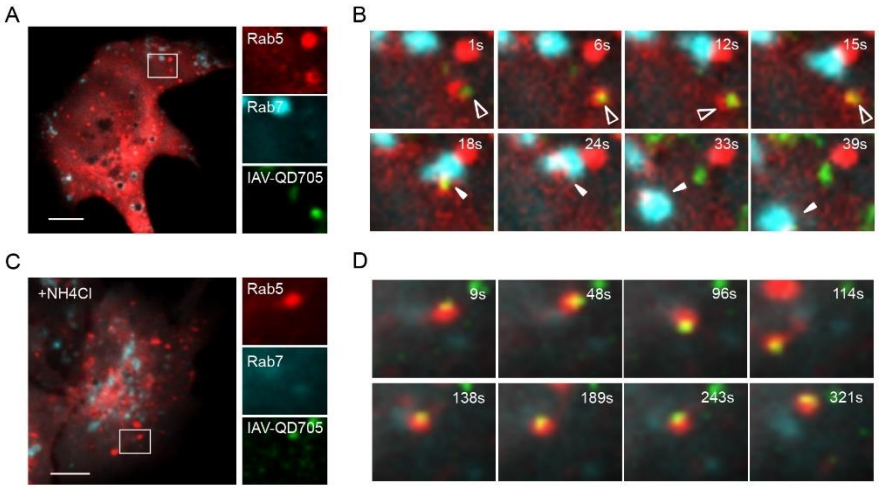

Fig. S4. Real-time imaging of IAV-QDs transport from Rab5- to Rab7-positive endosome. (*A*) IAV-QD705 (green) colocalization with an mCherry-Rab5-positive endosome (red) in a host cell was tracked. Scale bar: 5 μm. (*B*) Sequential snapshots are shown for the transport of IAV-QD705 from Rab5 signal and Rab7 signal (cyan) in the rectangular region of (*A*). Hollow arrowheads indicate colocalization of QD and Rab5 signals. Filled arrowheads indicate the colocalization of QD and Rab7 signals. (*C*) Fluorescence image of an infected cell treated with NH_4Cl. Scale bar: 5 μm. (*D*) Sequential images of the rectangular region of (*D*).

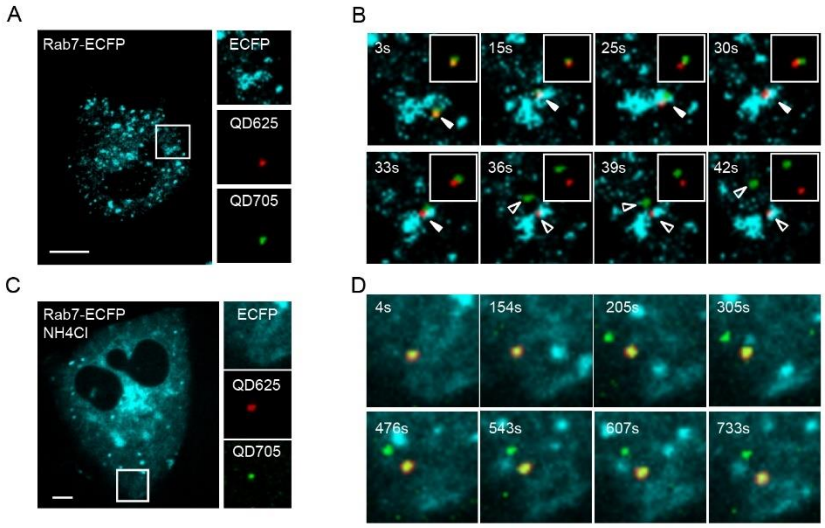

Fig. S5. Real-time imaging of dual-color IAV virions fusion and penetration from Rab7-positive endosomes. (*A*) Dual-color IAV virion (QD625-envelope, red and QD705-vRNP, green) colocalization with an ECFP-Rab7-positive endosome (cyan) in a host cell was tracked. Scale bar: 5 μm. (*B*) Sequential snapshots are shown for the separation of the QD705-vRNP signal from Rab7 signal and QD625-envelope signal in the rectangular region of (*A*). Filled arrowheads indicated the virion located in Rab7-endosome, hollow arrowheads indicated penetration of QD705-vRNP from Rab7-endosome. Unmerged panels for dual-color IAV virion were inserted in right region with white boundary. (*C*) Fluorescence image of an infected cell treated with NH_4Cl. Scale bar: 5 μm. (*D*) Sequential images of the rectangular region of (*C*).

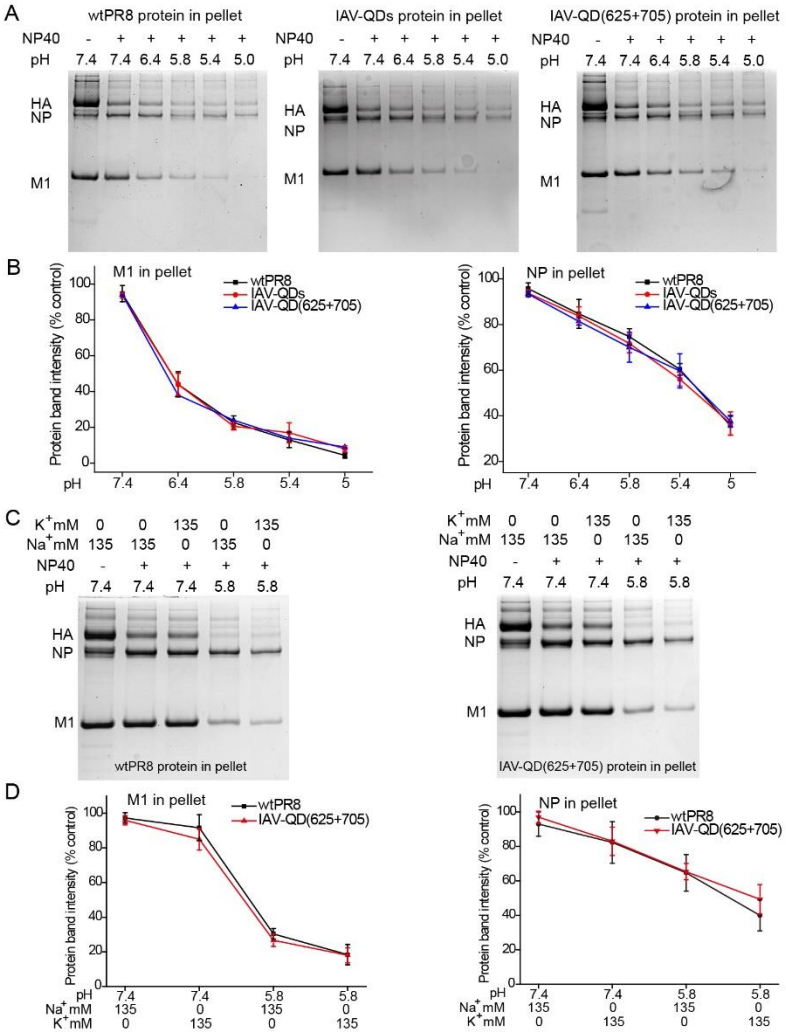

Fig. S6. *In vitro* assay of virion stability. (*A*) In vitro disassembly of wtPR8, IAV-QDs and IAV-QD(625+705) under different pH condition. (*B*) Densitometric quantification of the intensities of viral protein bands (M1 and NP) shown in (*A*). (*C*) Effect of a high K^+ concentration (135 mM) and pH 5.8 on wtPR8 and IAV-QD(625+705) uncoating *in vitro*. (*D*) Densitometric quantification of the intensities of viral protein bands (M1 and NP) of wtPR8 and IAV-QD(625+705) on high K^+ concentration (135 mM) and pH 5.8. Protein band intensities were normalized to samples at pH7.4 without NP-40.

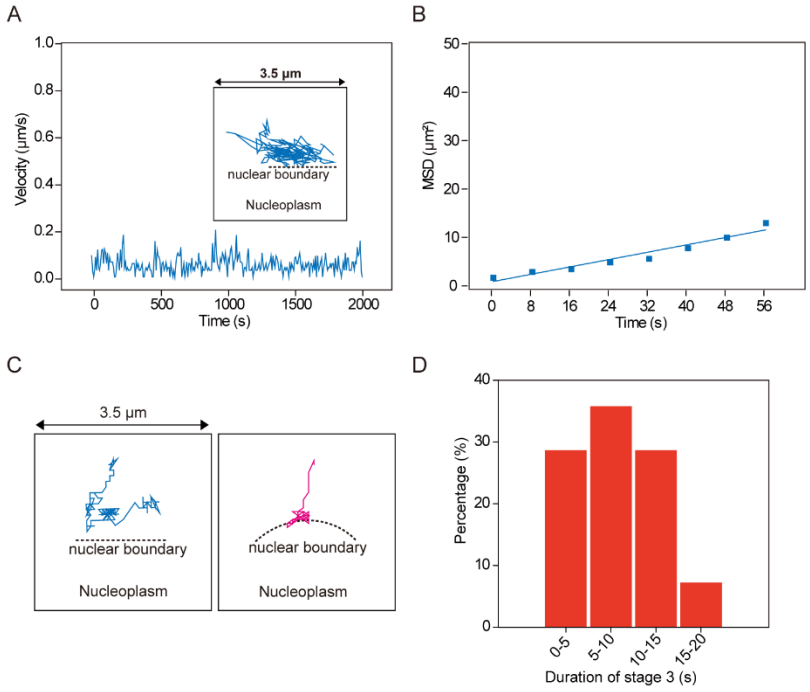

Fig. S7. Characterization of QD-vRNPs that failed to enter the nucleus. (*A*) Analysis of velocities of the QD-vRNPs that failed at nuclear entry. (*B*) MSD plots of the QD-vRNPs in (*A*). (*C*) Trajectories of two forms of QD-vRNPs that failed at nuclear entry. (*D*) Histogram of the duration of stage 3.

Movie S1 Real-time imaging of the cytoplasmic movement of an individual IAV-QD virion. MDCK cells were infected with IAV-QDs. Fluorescence was imaged with an UltraView Vox spinning disk confocal laser scanning system (PerkinElmer, Co.). Sequential images were taken at 3-s intervals for 14 min and 51 s, and the movie frame rate is 30 frames per second (fps). The trajectory of an IAV-QD particle on a MDCK cell is shown in the movie. This particle was adsorbed to the cell membrane at the beginning, and its trafficking from the cytoplasm to the perinuclear region was recorded. Scale bar: 2 μm.

Movie S2 Real-time imaging of the cytoplasmic-to-nuclear movement of an individual IAV-QD virion. MDCK cells with Nup153-Venus-labeled nuclear membranes were infected with IAV-QDs. Sequential images were taken at 3-s intervals for 50 min and 40 s, and the movie frame rate is 30 frames per second (fps). The trajectory of an IAV-QD particle on a MDCK cell is shown in the movie. The processes of cytoplasmic transport, nuclear entry, and intranuclear trafficking were captured in this move. Scale bar: 10 μm.

Movie S3 Real-time imaging of IAV uncoating by dual-color visualization in live cells. MDCK cells were infected with dual-color IAV virions (QD525 viral surface decoration of IAV-QD625). Sequential images were taken at 3.5-s intervals for 3 min and 48 s, and the movie frame rate is 20 frames per second (fps). The trajectory of a dual-color IAV

particle on a MDCK cell is shown in the movie. The co-localized QD signal was tracked, the QD625 signal (red) was separated from the QD525 signal (cyan) at the perinuclear region. Scale bar: 2 μm.

Movie S4 Real-time imaging of amantadine inhibition of IAV uncoating in live cells. After pretreatment with amantadine for 1 h, MDCK cells were infected with dual-color IAV virions (QD525 viral surface decoration of IAV-QD625). Sequential images were taken at 1.5-s intervals for 24 min and 28 s, and the movie frame rate is 20 frames per second (fps). The trajectory of a dual-color IAV particle on a MDCK cell is shown in the movie. The separation event of this co-localized QD signal did not happen at the perinuclear region. Scale bar: 2 μm.

Movie S5 Real-time imaging of vRNP release from a Rab7-positive endosome in live cells. MDCK cells with Rab7-ECFP-labeled late endosomes were infected with IAV-QDs. Sequential images were taken at 2.2-s intervals for 31 min and 57 s, and the movie frame rate is 30 frames per second (fps). The trajectory of an IAV-QD particle with late endosomes on a MDCK cell is shown in the movie. The QD signal (red) initially overlapped with the signal from the late endosome marker Rab7 (cyan), after which they were transported together from the cytoplasm to the perinuclear region, and the red signal was finally released from the cyan signal in the perinuclear region. Scale bar: 2 μm.

Movie S6 Real-time imaging of NH_4Cl inhibition of vRNP release from a Rab7-positive endosome in live cells. MDCK cells with Rab7-ECFP-labeled late endosomes were infected with IAV-QDs. Sequential images were taken at 2.3-s intervals for 12 min and 9 s, and the movie frame rate is 30 frames per second (fps). The trajectory of an IAV-QD particle on a MDCK cell is shown in the movie. IAV-QD virions rarely colocalized with Rab7-endosomes. Scale bar: 2 μm.

Movie S7 Real-time imaging of NH_4Cl inhibition of IAV-QDs transport from Rab5- to Rab7-positive endosome in live cells. MDCK cells with co-expression of Rab5-mCherry-labeled early endosome and Rab7-ECFP-labeled late endosomes were infected with IAV-QDs. Sequential images were taken at 3-s intervals for 5 min and 21 s, and the movie frame rate is 30 frames per second (fps). The representative trajectory of an IAV-QD particle on a MDCK cell is shown in the movie. The IAV-QD virion was trapped in Rab5-endosomes. Scale bar: 2 μm.

Movie S8 Real-time imaging of dual-color IAV virions fusion and penetration from Rab7-positive endosomes in living cells. MDCK cells with Rab7-ECFP-labeled late endosomes were infected with dual-color IAV virions. Sequential images were taken at 3-s intervals for 39 s, and the movie frame rate is 20 frames per second (fps). The representative trajectory of a dual-color IAV virion on a MDCK cell is shown in the movie. The dual-color IAV virion fused and vRNP penetrated from Rab7-endosome. Scale bar: 2 μm.

Movie S9 Real-time imaging of NH_4Cl inhibition of dual-color IAV virions fusion and penetration from Rab7-positive endosomes in living cells. MDCK cells with Rab7-ECFP-labeled late endosomes were infected with dual-color IAV virions. Sequential images were taken at 1.8-s intervals for 15 min and 49 s, and the movie frame rate is 50 frames per second (fps). The representative trajectory of a virion particle on a MDCK cell is shown in the movie. The dual-color IAV virion rarely colocalized with Rab7-endosomes. Scale bar: 2 μm.

Movie S10 Real-time imaging of IAV vRNP separation into individual parts at the AN region. MDCK cells were infected with IAV-QD(625+705). Sequential images were taken at 3.5-s intervals for 13 min and 39 s, and the movie frame rate is 30 frames per second (fps). The trajectory of an IAV-QD(625+705) particle on a MDCK cell is shown in the movie. The QD signal was tracked, and the red signal (QD625) was released from the green signal (QD705) in the AN region. Scale bar: 2 μm.

Movie S11 Real-time imaging of triple-color IAV virions sequential separation in living cells. MDCK cells were infected with triple-color IAV virions. Sequential images were taken at 4-s intervals for 2 min and 53s, and the movie frame rate is 20 frames per second (fps). The representative trajectory of a triple-color IAV virion on a MDCK cell is shown in the movie. QD625-vRNP and QD705-vRNP were separated from each other and released from QD525-envelope. Scale bar: 2 μm.

Movie S12 Real-time imaging of IAV vRNPs escaping from Rab7-positive endosomes. MDCK cells with Rab7-ECFP-labeled late endosomes were infected with IAV-QD(625+705). Sequential images were taken at 3.5-s intervals for 2 min and 22 s, and the movie frame rate is 20 frames per second (fps). The trajectory of an IAV-QD(625+705) particle with late endosomes on a MDCK cell is shown in the movie. The merged QD625 and QD705 fluorescent dots initially colocalized with the Rab7 fluorescent signals and then separated into two fluorescent dots moving away from the Rab7 signals, which moved in different directions for the next transportation stage. Scale bar: 2 μm.

Movie S13 Real-time imaging of vRNP nuclear import. MDCK cells with Hoechst33342-labeled nuclei were infected with IAV-QDs. Sequential images were taken at 1.5-s intervals for 7 min and 51 s, and the movie frame rate is 30 frames per second (fps). The trajectory of QD-vRNP nuclear import on a MDCK cell is shown in the movie. The QD signal (red) transported from the AN region to the nucleus with a three-stage transport pattern: the red signal moved from the AN region to the nucleus boundary, then associated with the nuclear membrane, and finally underwent rapid and unidirectional movement to arrive at its nuclear location. Scale bar: 5 μm.

SUPPORTING REFERENCES

1. Hoffmann E, Neumann G, Kawaoka Y, Hobom G, Webster RG (2000) A DNA transfection system for generation of influenza A virus from eight plasmids. Proc Natl Acad Sci USA 97:6108-6113.
2. Jeong J-Y, et al. (2012) One-step sequence- and ligation-independent cloning as a rapid and versatile cloning method for functional genomics studies. Appl Environ Microb 78:5440-5443.

3. Liu S-L, et al. (2012) Effectively and efficiently dissecting the infection of influenza virus by Quantum-Dot-based single-particle tracking. ACS nano 6:141-150.
4. Armstrong SJ, Dimmock NJ (1992) Neutralization of influenza virus by low concentrations of Hemagglutinin-specific polymeric immunoglobulin A inhibits viral fusion activity, but activition of the ribonucleoprotein is also inhibited. J Virol 66:3823-3832.
5. Hay AJ, Wolstenholme AJ, Skehel JJ, Smith MH (1985) The molecular-basis of the specific anti-influenza action of amantadine. Embo J 4:3021-3024.
6. Chou YY, et al. (2013) Colocalization of different influenza viral RNA segments in the cytoplasm before viral budding as shown by single-molecule sensitivity FISH analysis. PLoS pathog 9:e1003358.
7. Frensing T, et al. (2016) Influenza virus intracellular replication dynamics, release kinetics, and particle morphology during propagation in MDCK cells. Appl Microb Biot 100:7181-7192.
8. Stauffer S, et al. (2014) Stepwise priming by acidic pH and a high K+ concentration is required for efficient uncoating of influenza A virus cores after penetration. J Virol 88:13029-13046.